11 SCIENTIFIC HIGHLIGHT OF THE MONTH

Real-space relativistic spin-polarized photoemission

M. Woods[1], P. Strange[1], A. Ernst[2,3], and W. M. Temmerman[2]

[1]Department of Physics, Keele University, Staffordshire, ST5 5DY, England
[2]Daresbury Laboratory, Daresbury, Warrington WA4 4AD, England
[3]Max-Plank-Institut fur Mikrostukturphysik, Weinberg 2, D-06120 Halle, Germany

Introduction

It is now a routine matter to calculate band structures using the local density approximation (LDA) to Density Functional Theory (DFT). A full knowledge of the electronic structure is the key to understanding the solid state properties of a material. Experimentally, the probe of choice for determining the electronic structure on a band by band basis is angle-resolved photoemission spectroscopy (ARPES) [1]. The availability of a variable photon energy source in the form of synchrotron radiation has made angle-resolved photoemission into a practical and versatile tool in physics. Photoemission provides a convenient and much-used probe of the electronic properties [2]. The basis of this spectroscopy is the photoelectric effect in which the energy of an incident photon is transferred entirely to an electron of the irradiated material. If the energy of the incident photon is large enough for the electron to overcome the work function of the solid, the electron can escape the material and is detected by an electron spectrometer. In photoelectron spectroscopy the surface of the sample is irradiated by monochromatic light of energy $\hbar\omega$ and the kinetic energy of the emitted electrons is measured. Angle-resolved photoemission determines, as well as the energy, the emission angle of the photoelectrons and thus measures the external momentum. Finally, in spin- and angle-resolved photoemission the polarisation of the emitted electrons can also be analysed. These observables yield information about the binding energy E_B, the momentum $\mathbf{k}$, and the spin $\mathbf{s}$ of the electrons inside the solid. By proper choice of the angle and polarization of the incident radiation, the analysis of the obtained electron energy spectrum can be simplified enormously by the symmetry selection rules [3].

The need for a relativistic approach to the theory of photoemission is clear. Relativistic effects such as spin-orbit coupling, play a key role in the electronic structure of all materials, and this increases dramatically with atomic number. These effects were studied in pure metals by

McDonald *et al.* (1981) [4] and Fasol *et al.* (1988) [5] and in random alloys by Ginatempo and Staunton (1988) [6]. Strange (1998) [7] discusses relativistic effects in solids in general. All these calculations have their foundations in relativistic spin-density functional theory so any calculation that bridges the gap between first-principles energy bands and experimentally measured photoemission spectra is worthwhile.

For pure metals the framework for the required calculations of the photocurrent has already been developed. A quite general theory that includes ferromagnetic order on an equal footing with relativistic effects was put forward by Ackermann and Feder (1985a) [8]. A theory of energy-, angle- and spin-resolved photoemission spectroscopy of non-magnetic crystalline metals on the basis of relativistic quantum mechanics was written down first by Ginatempo *et al.* (1989) [9]. Here I present a derivation of the theory of relativistic spin-polarized photoemission based on the real-space Green's function method [10]. The real-space multiple scattering theory offers a fertile field of investigations of systems with arbitrary arrangements of atoms. It also has the advantage of a simple expression for the photocurrent in terms of site-off diagonal multiple scattering quantities and the site dependent matrix elements. This theory implements the real-space theory of Durham (1984) [11], within the framework of the one-step model of Pendry (1976) [2]. The formulation of the theory of photoemission discussed here builds on previous work. The underlying theory of photoemission is identical to that of Ebert and Schwitalla (1996)[12], however, their implementation was for bulk materials only. In the present formulation a real space implementation has been developed analogous to the non-relativistic theory of Ernst *et al.* (1998)[13]. This means that we can treat systems of low dimension, particularly surfaces and nanostructures easily.

Theory

The relativistic theory of photoemission is really an application of the first order Golden rule, giving the transition rate between the initial state $|i\rangle$ and the final state $|f\rangle$ due to a perturbation. For a single process this is

$$T = -\frac{2}{\hbar}\sum_f \int\int \psi_f^\dagger(\mathbf{r}) H'(\mathbf{r}) \mathrm{I}m\mathbf{G}^r(\mathbf{r},\mathbf{r}';\epsilon_i) H'^\dagger(\mathbf{r}) \psi_f(\mathbf{r}') d^3\mathbf{r}\; d^3\mathbf{r}' \tag{1}$$

where

$$H'(\mathbf{r}) = -ec\alpha\cdot\mathbf{A}(\mathbf{r}) \tag{2}$$

is the perturbation responsible for the transition and describes the electron-photon interaction. Here $\mathbf{G}^r(\mathbf{r},\mathbf{r}';\epsilon_i)$ is the retarded Green's function at energy ϵ, and ψ_f is the so called time reversed low-energy electron diffraction (LEED) state given by

$$\psi_f(\mathbf{r}) = \phi(\mathbf{r}) + \int \mathbf{G}^r(\mathbf{r},\mathbf{r}';\epsilon) V(\mathbf{r}')\phi(\mathbf{r}')\mathbf{dr}'. \tag{3}$$

which describes the final state of the electron. This equation follows from the asymptotic formula of the retarded Green's function. The retarded Green's function $\mathbf{G}^r(\mathbf{r},\mathbf{r}';\epsilon_i)$ in equation (1) can be calculated using the powerful technique of multiple-scattering theory. The crystal potential $V(\mathbf{r})$ is the total potential in the one-electron Dirac Hamiltonian taken to consist of an array of

non-overlapping muffin-tin potentials representing the lattice of atoms.

$$V(\mathbf{r}) = \sum_i v_i(\mathbf{r} - \mathbf{R}_i) \tag{4}$$

Accordingly we write the total potential as a sum over the lattice sites R_i where $v_i(\mathbf{r})$ is a muffin-tin potential at site i. Outside the muffin-tins a constant potential is assumed.

An essential feature of this approach is the use of the τ-matrix representation of multiple-scattering theory developed by Györffy and Stott [10] in which the retarded Green's function is defined as

$$G^r(\mathbf{r}, \mathbf{r}', \epsilon) = \sum_{\Lambda_1} \sum_{\Lambda_2} Z_{\Lambda_1}(\mathbf{r}; \epsilon) \tau^{ij}_{\Lambda_1 \Lambda_2}(\epsilon) Z^{\dagger}_{\Lambda_2}(\mathbf{r}'; \epsilon) - \sum_{\Lambda} Z_{\Lambda}(\mathbf{r}) J^{\dagger}_{\Lambda}(\mathbf{r}'; \epsilon) \quad (r < r') \tag{5}$$

The τ-matrix $\tau^{ij}_{\Lambda'\Lambda''}(\epsilon)$, is a site and κm_j decomposition of the total T-matrix at energy ϵ and the $Z_{\Lambda'}(\mathbf{r}; \epsilon)$ and $J_{\Lambda'}(\mathbf{r}; \epsilon)$ functions are the regular and irregular solutions of the Kohn-Sham-Dirac equation with the single-site muffin-tin potential $v(\mathbf{r})$. These can be expanded in terms of radial and angular components:

$$Z_{\Lambda'}(\mathbf{r}; \epsilon) = \sum_{\kappa''=\kappa', -\kappa'-1} \begin{pmatrix} g^{m_j{}'}_{\kappa''\kappa'}(\mathbf{r}) \chi^{m_j{}'}_{\kappa''}(\hat{\mathbf{r}}) \\ i f^{m_j{}'}_{\kappa''\kappa'}(\mathbf{r}) \chi^{m_j{}'}_{-\kappa''}(\hat{\mathbf{r}}) \end{pmatrix} \tag{6}$$

and

$$J_{\Lambda}(\mathbf{r}; \epsilon) = \sum_{\kappa'=\kappa, -\kappa-1} \begin{pmatrix} g^{m_j \mathbf{i}}_{\kappa'\kappa}(\mathbf{r}) \chi^{m_j}_{\kappa'}(\hat{\mathbf{r}}) \\ \\ i f^{m_j \mathbf{i}}_{\kappa'\kappa}(\mathbf{r}) \chi^{m_j}_{-\kappa'}(\hat{\mathbf{r}}) \end{pmatrix}. \tag{7}$$

where the $\chi^{m_j}_{\kappa}$ are the usual relativistic spin-angular functions. Using equation (5) for the retarded Green's function with $r < r'$ in the Dyson equation (3) the time-reversed LEED state takes the following convenient form:

$$\psi_f(\mathbf{r}) = \frac{4\pi}{\sqrt{V}} \left(\frac{W + mc^2}{2W} \right)^{1/2} \sum_{\kappa m_j} (-i)^l C(l \tfrac{1}{2} j; m_j + m_s \ -m_s) Y_l^{m_j - m_s}(-\hat{k}) \sum_j e^{ik \cdot R_j} \sum_{\Lambda} \tau^{ij*}_{\Lambda'\Lambda}(\epsilon) \left[\hat{\tau} Z_{\Lambda'}(\mathbf{r}; \epsilon) \right] \tag{8}$$

where $C(l \frac{1}{2} j; m_j + m_s, -m_s)$ is a Clebsch-Gordon coefficient, $Y_l^{m_j + m_s}(-\hat{k})$ is a complex spherical harmonic, and $\hat{\tau}$ is the time-reversal operator. W is the total energy, including the rest mass energy. Equation (9) is the expression for the final state of the electron after photoemission.

Using the τ representation of the retarded Green's function (5) and equation (9) in (1), the photocurrent can be given as a sum of the inter-site contribution $M_{ij}(\epsilon + \hbar\omega)$, and the intra-site contribution $I_i(\epsilon + \hbar\omega)$:

$$T = \sum_{ij} M_{ij}(\epsilon + \hbar\omega) + \sum_i I_i(\epsilon + \hbar\omega). \tag{9}$$

The separation of the photocurrent equation into two contributing terms is done for convenience only because the intra-atomic term $I_i(\epsilon + \hbar\omega)$ vanishes for real energies and need not be calculated in this case. Thus we have obtained a fully relativistic photocurrent formula which is valid for any atomic arrangement. In essence we need to solve the multiple-scattering problem, that is

to find the single-site solution for the t-matrix, and the τ-matrices for low and high energies, which can be done using many well known methods.

One approach is the real-space cluster method for evaluating (5) and (9). In this case the τ-matrix can be obtained by inversion of the KKR matrix:

$$\underline{\tau}(\epsilon) = [\underline{t}^{-1}(\epsilon) - g_0(\epsilon)]^{-1} \tag{10}$$

For sufficient accuracy to describe real surfaces one usually needs to take into account a sufficiently large cluster. Our experience has been that we require at least about 100 atoms, because of the long range behaviour of the structure constants.

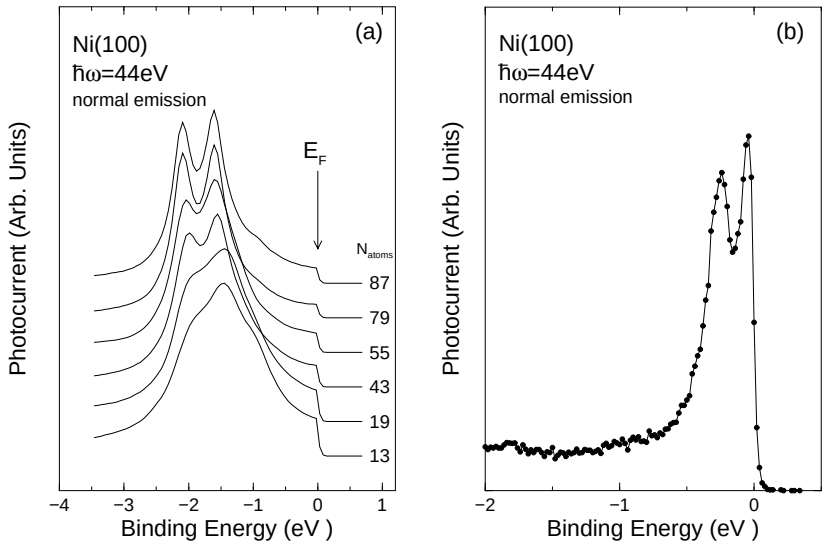

Figure 1: Photoemission spectrum of Ni(100). (a) Calculated photoemission spectra from different sized fcc configured clusters of atoms. (b) Experimental photoemission spectrum of Ni(100).

Figure 1 shows the convergence of the angle-resolved photocurrent for incident light of $\hbar\omega$=44.0 eV as a function of the size of cluster. Our calculations have been performed with broadening in the energy of 0.01 Ryd. What is evident is that the main features of the experiment (Figure 1(b)) are revealed by a relatively small cluster of 45 atoms but the Bloch State appears when the features no longer shift in energy ϵ which occurs with a cluster size of 87 atoms. The photocurrent for the cluster of 87 atoms is closer to the experiment but in this case the KKR-matrix is large, approximately 2800×2800, and needs 1.5 hours of CPU on a Dec Alpha 500 Series for the inversion of one energy point [14]. However with the inversion completed, the photocurrent for all θ and φ angles can be calculated without any further matrix inversion.

Calculations for Iron metal

Iron is an excellent metal to test relativistic theories because we have a reliable potential that reproduces experiment for Magnetic X-ray Circular Dichroism in absorption [15]. We have performed photoemission calculations on a cluster of 55 iron atoms where all atoms are described by identical bulk potentials. Clearly this takes into account surface geometry but neglects

changes in the potential due to the closeness of the surface. This is not a necessary restriction, but is done in this case for illustrative purposes only.

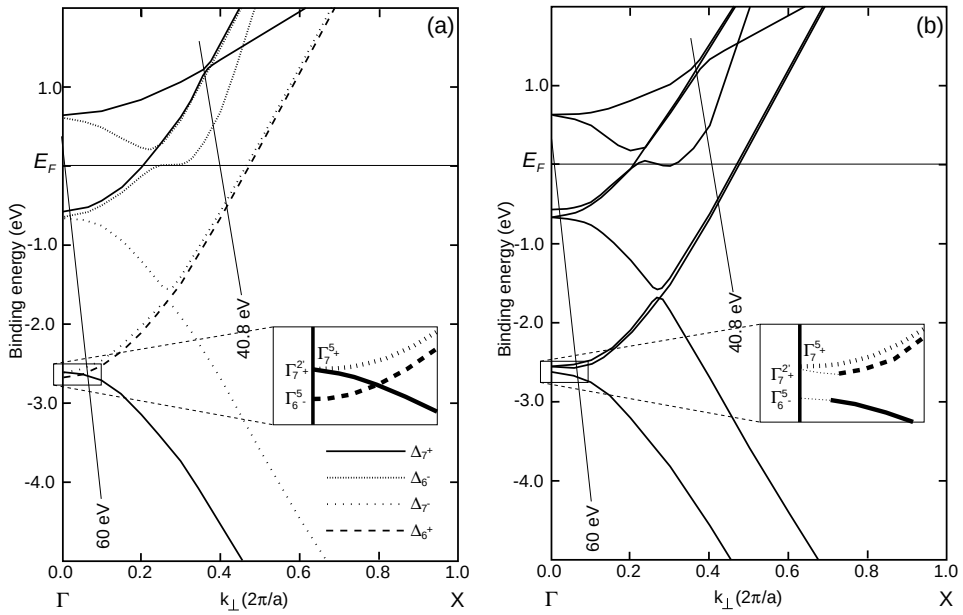

Figure 2: Symmetry resolved valence band structure of Fe(001). Bands with $\Delta_7+, \Delta_6+, \Delta_7-$ and Δ_6- double point group symmetry are distinguished as labelled in the figure. The thin solid lines are sections of the final state band, shifted down by the indicated photon energy. (b) as in (a) but for the Fe(100) direction.

Figure 2 shows the symmetry resolved band structure for Fe along two perpendicular directions of the Brillouin zone. Panel (a) shows the (001) direction with perpendicular magnetism. Panel (b) shows the (100) direction where the magnetic moment is oriented in plane. The (near) vertical solid lines are sections of the final state band shifted down by the energies used in the calculations. This clearly indicates the allowed transitions. At Γ the bands are identical in both figures of course. At Γ the band structure yields values for the exchange splitting of 2.1 eV and the crystal field splitting between the majority spin bands is 3.3 eV. The inset boxes in figure (1) not only show up the spin-orbit splitting at Γ but also clarify the differences in the band structure in the different directions as we proceed away from Γ. The differences in the bands are due to the subtle interplay between spin-orbit coupling and the magnetisation.

In figure (2) we observe the spin-resolved photoemission spectra attained with a 60 eV photon incident normal to the Fe(001) and Fe(100) surfaces. Incident radiation of this frequency probes the Brillouin zone close to Γ. Following Kuch *et al*[16] right and left circularly polarised incident photons will produce an asymmetry that is of use in determining the spin-orbit and magnetic anisotropy in local regions of k-space. Panel (a) decomposes the total photocurrent (solid line) generated with right circularly polarised photons into minority (dashed line) and majority (dotted line) spin contributions. Clearly the peak at -0.65 eV binding energy identifies transitions from the Δ_6^5+ band with a predominantly minority spin character. The peak at -2.5 eV marks transitions from the majority Δ_7^5- band. Panel (b) shows similar spectra attained with left circularly polarised incident radiation. This time the features mark transitions from Δ_6^5- at -2.6 eV and Δ_7^5+ at -0.55 eV. The total emission curves from panels (a) and (b) are brought

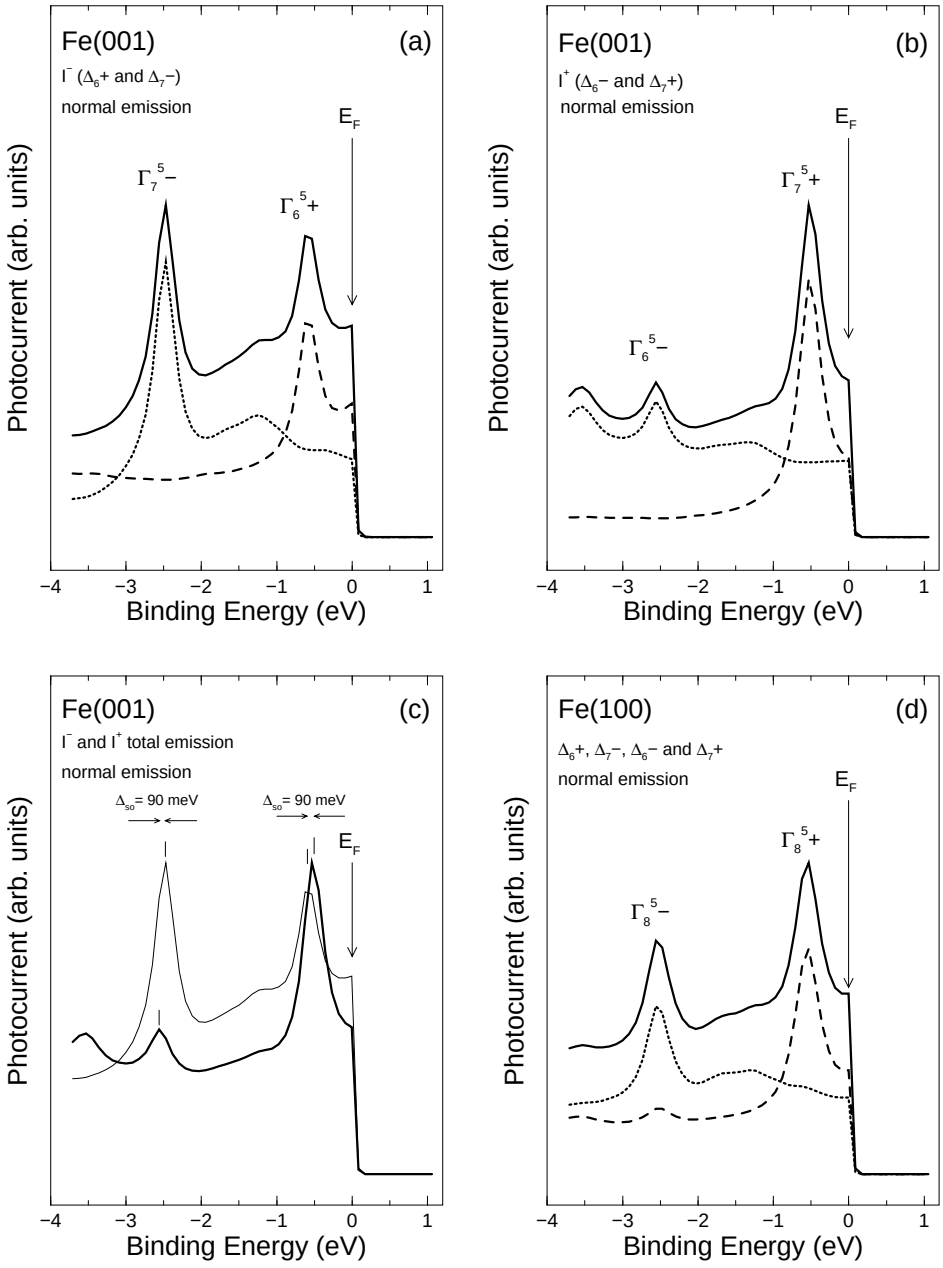

Figure 3: Spin-resolved photoemission spectra obtained with 60eV photons incident normal to the Fe(001) (perpendicular magnetisation) and Fe(100) (in-plane magnetisation). The calculations were performed with the same input parameters as used to calulcate the band structure of figure 2. Solid lines represent total emission and dashed (dotted) lines represent contributions from minority (majority) spin channels. (a) Right circularly polarised incident photons at the (001) surface. (b) Left circularly polarised photons incident at the (001) surface. (c) Assymetry between the totla spectra from panels (a) and (b) yielding the spin-orbit splitting. (d) Spin-resolved photoemission from the Fe(100) surface.

together in panel (c) and the spin-orbit splitting of 90 meV can be clearly seen.

We can compare the spectra probing close to Γ in both the (001) and (100) geometries. The in-plane magnetisation in the (100) case means there is no dichroism at normal incidence, the total photocurrent, and spin decomposed photocurrent for light incident normal to the Fe(100) surface is shown in panel (d). Comparison of the peak positions in panels (c) and (d) yields an energy shift of 50 meV. Similarly, at around -0.5 eV there is an energy difference of 50 meV due to the minority spin band with approximate Δ_6^5- symmetry shifting upwards and swapping places with the Δ_7^5- like band at Γ.

Figure (1) illustrates a common feature of band structures calculated relativistically, the avoided crossings at $k_\perp \approx 0.3(2\pi/a)$. At such points the bands may change their spin character, and consequently cannot be ascribed a spin label. Such points will yield common features in both the majority and minority spin photoemission spectra and identification of these points in the photoemission spectra with such band features should be straightforward.

Summary

We have reported on the development of a real-space fully-relativistic spin- and angle-resolved photoemission code in the independent particle approximation. The code takes potentials generated elsewhere and puts them into a geometry of choice. The method underlying this development is formulated in terms of multiple scattering theory with the real-space representation of the Green's function. The multiple scattering part in the photocurrent formula is separated from the angle-dependent part, leading to an essential simplification of the photocurrent calculations. The photocurrent formula is general and can be easily adapted to the symmetry of the problem at hand. The code is user friendly and yields results that can be used to give an easy handle on the main features of the photoemission spectra. The computations are limited by the size of the cluster that may be treated.

ACKNOWLEDGEMENTS

We thank E. Arola and F.J. Himpsel for many useful discussions.

References

[1] P. J. Durham, J. Phys. F: Metal Phys. **11**, 2475 (1981)

[2] J. B. Pendry, Surface Science, **57**, 679 (1976)

[3] R. Klasges, *Magnetism and quantum-size effects of thin fcc films*, *Thesis*, University of Koln, (1998)

[4] A. H. McDonald, J. M. Daams, S. H. Vosko, and D. D. Koelling, Phys. Rev. B **23**, 6377 (1981)

[5] G. Fasol, N. E. Christensen, and M. Cardona, Phys. Rev. B **38**, 1806 (1988)

[6] B. Ginatempo and J. B. Staunton, J. Phys. F: Metal Phys. **18**, 1827 (1988)

[7] P. Strange, *Relativistic Quantum Mechanics*, Cambridge University Press, (1998)

[8] B. Ackermann and R. Feder, J. Phys. C: Solid State Phys. **18**, 1093 (1985a)

[9] B. Ginatempo, P. J. Durham and B. L. Györffy, J. Phys.: Condens. Matter **1**, 6483 (1989)

[10] B. L. Györffy and M. J. Stott, in *Band Structure Spectroscopy of Metals and Alloys*, NATO edited by D. J. Fabian and L. M. Watson, Academic, New York, p. 385 (1973)

[11] P. J. Durham, *The Electronic Structure of Complex Systems*, NATO ASI Series B: Physics Vol. 113 edited by P. Phariseau and W. M. Temmerman, 709 (1984)

[12] H. Ebert and J. Schwitalla, Phys. Rev. B **55** 3100, (1996).

[13] A. Ernst, W. M. Temmerman, Z. Szotek, M. Woods and P. J. Durham, Phil. Mag. B: **78**, 503-511 (1998)

[14] *Harwell Subroutine Library*, AEA Technology, Harwell Laboratory, Oxfordshire, England, (1997)

[15] H. Ebert, P. Strange and B.L. Gyorffy, *Journal of Applied Physics*, **63**, 8, 3055, (1988)

[16] W. Kuch, M. Zharnikov, A. Dittschar, K. Meinel, C. M. Schneider, J. Kirschner, J. Henk and R. Feder, Phys. Rev. B **53**, 11621 (1995)